Journal of Physics: Conference Series **2533** (2023) 012031 doi:10.1088/1742-6596/2533/1/012031

Analog simulations of early universe pre-heating and the back-reaction effect

Salvatore Butera

School of Physics and Astronomy, University of Glasgow, Glasgow G12 8QQ, UK

E-mail: salvatore.butera@glasgow.ac.uk

Iacopo Carusotto

Pitaevskii BEC Center, CNR-INO and Dipartimento di Fisica, Università di Trento, I-38123 Trento, Italy

E-mail: iacopo.carusotto@unitn.it

Abstract. We theoretically propose a ring-shaped, two-dimensional atomic Bose-Einstein condensate as analog model to investigate back-reaction effects during the pre-heating of the early universe. We study the out-of-equilibrium dynamics by which the inflaton field decays by parametrically exciting the vacuum fluctuations that initially populate the matter fields. By working at the level of the truncated Wigner approximation, our numerical simulations show how a signature of back-reaction beyond the semiclassical level is encoded in the effective friction experienced by the analog of the inflaton field, as well as in the spatial de-phasing of its oscillations and in the entanglement between the inflaton and matter fields degrees-of-freedoms.

1. Introduction

Analog models of gravity are a powerful platform where a wide range of effects of quantum fields in curved spacetime can be studied from first principles and potentially find experimental confirmation [1]. The past few decades have seen remarkable advances in the field, resulting in a surge of both theoretical and experimental works investigating different phenomena with a multitude of analog configurations (see topical reviews [2, 3], and references therein). Experimentally, exceptional results have been achieved leading to the pioneering observation of the Hawking radiation [4, 5] emanating from a sonic black hole [6, 7, 8] implemented in trans-sonically flowing Bose-Einstein condensates (BECs) of ultra-cold atoms [9, 10], as well as to the observation of cosmological particle creation both in a BEC [11] and in quantum fluids of light [12], and the detection of superradiant scattering induced by a rotating sonic black holes, implemented in a water tank exhibiting a draining vortex flow configuration [13].

The next challenge that stands in front of the analog gravity community is to extend these investigations to the so-called *back-reaction* effect [14], thus widening the objectives of the field beyond the standard test-field level of quantum fields in curved spacetime and address the role of the mutual, that is two-way, interaction between spacetime and quantum fields. Clarifying this interplay is of fundamental importance in gravity to gain a deeper understanding of those physical configurations characterized by strong gravitational interactions, in which quantum effects are important. Pioneering studies have in fact anticipated that quantum effects may

have had a profound influence in driving the evolution of the early universe towards the present stage [15, 16, 17, 18, 19]. Related to this, black holes are expected to evaporate and eventually disappear due to the emitted Hawking radiation [4, 5]. Despite the amount of work carried out since the 1970's (see for example [20]), a clear picture of the physical processes involved in the back-reaction are still far from being clearly understood. The main reason is that a detailed understanding of the microscopic dynamics of spacetime is missing and only alternative top-down approaches, which attempt to include quantum fluctuations starting from the macroscopic level of the classical theory of general relativity, can be pursued [21].

To circumvent this fundamental difficulty, toy models characterized by a lower number of degrees-of-freedom have been extensively exploited in the literature, with the aim of capturing at least the main qualitative features of the back-reaction. For example, by using a zero-dimensional model for a black hole and by pursuing a fully quantum treatment of the problem, the deviation from thermal spectrum of the (analog of) Hawking radiation has been predicted [22, 23]. Similarly, in optomechanics, theoretical studies have anticipated a radiative friction experienced by an accelerated mirror in response to the dynamical Casimir emission (DCE) [24, 25, 26], and hinted at an important role of quantum fluctuations in determining the evolution of the quantum state of the mirror itself [27, 28, 29, 30].

Analog systems represent a promising platform where back-reaction effects can be investigated in the framework of quantum fields interacting with an effective background spacetime, thus retaining the full multi-mode character of the problem [31, 32]. On the one side, these systems bring the unprecedented capability to perform table-top experiments where these effects manifest in observable physical systems. On the other side, the in depth knowledge of the microscopic dynamics of these systems permits, at least in principle, the development of a self-consistent theoretical description of the problem starting from first principles. Even though the microscopic dynamics of analog systems is expected to be different from the (still unknown) physics of spacetime at the Planck scale, crucially, the mesoscopic observable effects of the back-reaction such as *fluctuation*, *dissipation* and *decoherence* are expected to be universal, since they result from a coarse-graining process, and are thus ultimately insensitive to the details of the microscopic physics. The basic mechanisms that drive the back-action of quantum fields are thus qualitatively the same, independently whether the underlying spacetime is physical (in the case of gravity) or effective (in the case of analogue systems). This assumption is well-established and is at the basis of effective field theories [33].

In this paper we study the back-reaction by considering an analog model of the pre-heating of the early Universe [34] inspired to the proposal in [35]. Our work substantially extends the short presentation recently appeared in [36]. According to the inflationary model, pre-heating is the last stage of cosmic inflation, when the inflaton field that drives the primordial exponential expansion of the universe reaches the end of its potential plateau and starts oscillating around the minimum of the potential well. Matter is thus created in the still empty universe out of the zero-point fluctuations of the matter fields, due to the parametric processes induced by the inflaton oscillations. In our analog model, we simulate this mechanism by using an elongated BEC as a platform, that we take as two-dimensional for numerical ease. Specifically, we identify the inflaton degrees-of-freedom with the relatively high energy transverse modes of the system, and the matter degrees-of-freedom with the lower energy longitudinal modes. We simulate the inflaton oscillations around its potential minimum by exciting the breathing mode of the system in the transverse direction and study the mechanism that leads to the parametric excitation of vacuum fluctuations in the longitudinal modes. By working with this quantum simulator, we aim to clarify key non-equilibrium processes by which energy is transferred from the transverse modes into the longitudinal modes, focusing on back-reaction effects. In the spirit of analog simulators and by working within the analogy described above, we expect that our results reveal the key qualitative features of the corresponding processes taking place in an actual cosmological

scenario.

2. Bogoliubov theory

We perform our analog simulations by considering a dilute two-dimensional Bose gas of mass m atoms at zero temperature, whose many-body Hamiltonian reads [37]:

$$\hat{H} = \int d\mathbf{r} \left[\hat{\Psi}^\dagger(\mathbf{r}) \hat{h} \hat{\Psi}(\mathbf{r}) + \frac{U}{2} \hat{\Psi}^\dagger(\mathbf{r}) \hat{\Psi}^\dagger(\mathbf{r}) \hat{\Psi}(\mathbf{r}) \hat{\Psi}(\mathbf{r}) \right]. \tag{1}$$

Here, $\hat{h} \equiv -(\hbar^2/2m)\boldsymbol{\nabla}^2 + V_{\rm ext}(\mathbf{r})$ is the quantum mechanical single particle Hamiltonian, where $\boldsymbol{\nabla} \equiv d/d\mathbf{r}$ the standard *nabla* operator, $V_{\rm ext}(\mathbf{r})$ is an external potential, and $\hat{\Psi}(\mathbf{r})$ is the bosonic many-body field operator which obeys the equal time commutation rule: $[\hat{\psi}(\mathbf{r}), \hat{\psi}^\dagger(\mathbf{r}')] = \delta(\mathbf{r}-\mathbf{r}')$. The last terms in Eq. (1) accounts for a zero-range collisional interaction between atoms, whose strength we indicated by U. The Heisenberg equation for the field operator $\hat{\Psi}(\mathbf{r}, t)$ is readily obtained in the form:

$$i\hbar \frac{\partial \hat{\Psi}}{\partial t} = [\hat{\Psi}, \hat{H}] = \left(\hat{h} + g \hat{\Psi}^\dagger \hat{\Psi} \right) \hat{\Psi}. \tag{2}$$

By following the number conserving Bogoliubov formalism developed in [38, 39], we split the field operator $\hat{\Psi}(\mathbf{r}, t)$ into the *condensed* component describing atoms occupying the single particle ground state, and the *non-condensed* component that accounts for the population of the excited single-particle states:

$$\hat{\Psi}(\mathbf{r}, t) = \phi_0(\mathbf{r}, t) \hat{a}_0 + \delta\hat{\Psi}(\mathbf{r}, t). \tag{3}$$

Here the operator $\hat{a}_0$ annihilates a particle from the condensate mode $\phi_0(\mathbf{r}, t)$, while $\delta\hat{\Psi}(\mathbf{r}, t)$ annihilates a non-condensed particle at position $\mathbf{r}$. In the weakly-interacting regime, identified by the limit of large number of particles $N \to \infty$, and vanishing coupling constant $U \to 0$ (with the mean field interaction strength $U_N \equiv UN$ kept constant), a perturbative description for the system can be pursued [38] with respect to the parameter $\delta N/\sqrt{N}$, with

$$\delta N \equiv \int d\mathbf{r} \left\langle \delta\hat{\Psi}^\dagger(\mathbf{r}) \delta\hat{\Psi}(\mathbf{r}) \right\rangle \tag{4}$$

the number of particles in the excited single-particles states outside the condensate. The value of δN is set by the mean field interaction strength U_N and is of order $\delta N \sim \mathcal{O}(1)$, while N is macroscopic in the limit discussed above. Upon substitution of Eq. (3) into Eq. (2), the leading term of order $\mathcal{O}(\sqrt{N})$ gives the Gross-Pitaevskii equation (GPE), that governs the dynamics of the order parameter $\phi_0(\mathbf{r}, t)$. This reads:

$$i\hbar \frac{\partial \phi_0}{\partial t} = \left(\hat{h} + |\phi_0|^2 \right) \phi_0 \equiv \hat{H}_{GP} \phi_0. \tag{5}$$

The term of order $\mathcal{O}(1)$ in Eq. (2), that is linear in the quantum fluctuations describes the non-interacting dynamics of the elementary excitations in the system. Such excitations are described by the operator $\hat{\Lambda}(x) \equiv \frac{1}{\sqrt{N}} \hat{a}_0^\dagger \delta\hat{\Phi}(x)$ that transfers a particle from the non-condensed into the condensate component, and obeys the Bogoliubov-de Gennes equations [38]:

$$i\hbar \frac{d}{dt} \begin{pmatrix} \hat{\Lambda} \\ \hat{\Lambda}^\dagger \end{pmatrix} = \mathcal{L}_{\rm BdG}[\phi_0, \phi_0^*] \begin{pmatrix} \hat{\Lambda} \\ \hat{\Lambda}^\dagger \end{pmatrix}, \tag{6}$$

where the Bogoliubov operator is defined as:

$$\mathcal{L}_{\rm BdG}[\phi_0, \phi_0^*] = \begin{pmatrix} L_{QQ} & L_{QQ^*} \\ -L_{Q^*Q} & -L_{QQ} \end{pmatrix} \begin{pmatrix} \hat{\Lambda} \\ \hat{\Lambda}^\dagger \end{pmatrix} \tag{7}$$

with (operator-valued) components:

$$L_{QQ} = \left[\hat{H}_{\rm GP} + U_N\, Q|\phi_0(x,t)|^2 Q - \mu\right], \tag{8a}$$

$$L_{QQ^*} = N g_{1D}\, Q\phi_0^2(x,t) Q^*, \tag{8b}$$

$$L_{Q^*Q} = (L_{QQ^*})^* . \tag{8c}$$

Here $\hat{H}_{\rm GP}$ is the Gross-Pitaevskii Hamiltonian defined in Eq. (5), while the operator $Q \equiv \mathbb{I} - |\phi_0\rangle\langle\phi_0|$ is the projector onto the non-condensed component, that is onto the Hilbert subspace spanned by all single particle excited states.

The higher order [cubic $O(1/\sqrt{N})$ and quartic $O(1/N)$] terms in the quantum fluctuations, in the Hamiltonian Eq. (1), describe the self-interaction and scattering between Bogoliubov quasiparticles, and are responsible for back-reaction and thermalization processes. We will account for these term, and thus for the full nonlinear dynamics of the problem, by using the so-called truncated Wigner approximation which we introduce in Sec. 4.

3. Physical system

We consider a dilute two-dimensional Bose gas homogeneous along the longitudinal x direction with periodic boundary conditions and trapped in the transverse y direction by an external potential $V_{\rm ext}(\mathbf{r}) = V_{\rm ext}(y)$. For numerical convenience, this is taken as harmonic of frequency ω_0 at small y with a hard-wall at $y = \pm L_y/2$ on both sides. At zero temperature, most of the atoms in the system are condensed in the ground state, whose wave function $\varphi_0(\mathbf{r})$ is given by solving the stationary GPE, obtained from Eq. (5) by posing $\phi_0(\mathbf{r},t) = \varphi_0(\mathbf{r})\exp(-i\mu t/\hbar)$ [37]:

$$\hat{H}_{GP}\varphi_0(\mathbf{r}) = \mu\,\varphi_0(\mathbf{r}), \tag{9}$$

with μ the chemical potential of the cloud.

The spectrum $\{\omega_n^r\}$ of the collective Bogoliubov modes on top of the ground-state and the corresponding eigenfunctions $\{u_n^r, v_n^r\}$ are calculated by diagonalizing the Bogoliubov operator:

$$\mathcal{L}_{\rm BdG}[\varphi_0, \varphi_0^*] \begin{pmatrix} u_n^r \\ v_n^r \end{pmatrix} = \omega_n^r \begin{pmatrix} u_n^r \\ v_n^r \end{pmatrix}. \tag{10}$$

For each mode, the integer-valued subscript n and the superscript $r = g,\, d,\, b,\, ...$ respectively identify the longitudinal wave vector $k = 2\pi n/L_x$ and the different excitation branches, labelled by the number of transverse nodes in the wavefunction (g = Goldstone – 0 nodes; d = dipole – 1 node; b = breathing – 2 nodes). In Fig. 1(a), we show the three lowest excitation bands for the two set of system parameters used throughout this work. The transverse profiles of the real part of the $u_0^r(y)$ functions of the $k = 0$ modes of the three $r = g, d, b$ branches are displayed in Fig. 1(b). Along the longitudinal x direction, thanks to translational invariance, each mode has a plane-wave shape.

As an explicit check of our numerical calculations, throughout this work we compare the predictions relative to a system composed by $N = 10^6$ atoms, of longitudinal(transverse) length $L_x = 140\ell_0$ ($L_y = 3.54\ell_0$) (with $\ell_0 \equiv \sqrt{\hbar/2m\omega_0}$ the transverse harmonic oscillator length) and number of grid points in the longitudinal(transverse) direction $N_x = 512$ ($N_y = 12$), with the corresponding results obtained for a system composed by $N = 750,000$ atoms, of equal transverse size but of longitudinal length $L_x = 105\ell_0$ and corresponding number of grid points $N_x = 384$. We used a different number of longitudinal grid-points in order keep constant the grid spacing δl, to the value $\delta l \approx 0.4\xi$, where $\xi = \hbar/\sqrt{2m\mu}$ is the healing length. In order to reproduce the same physical conditions and show that the results reported in the following are

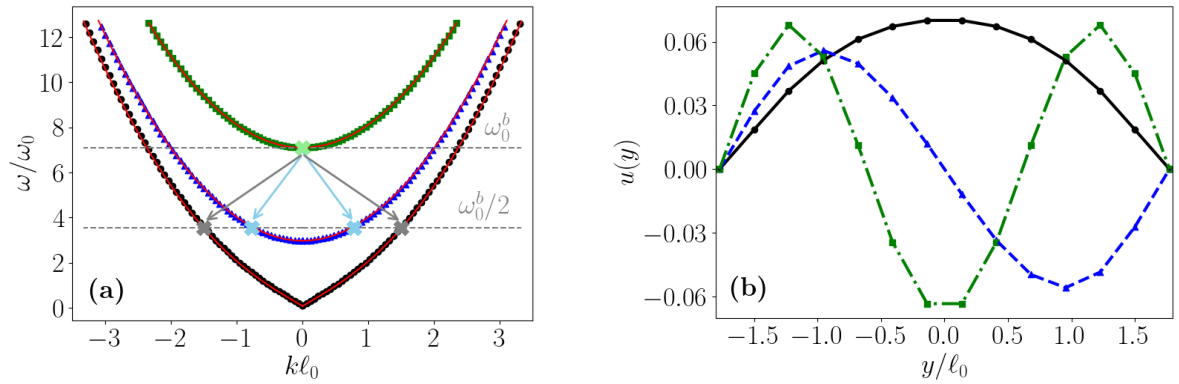

Figure 1. (a) Bogoliubov spectrum of collective excitations on top of the ground state of the system. Coloured markers provide the solution for a gas of $N = 10^6$ atoms in an integration box of size $L_{x,y}/\ell_0 = 140, 3.54$ in units of the transverse harmonic oscillator length $\ell_0 = \sqrt{\hbar/2m\omega_0}$, with $N_{x,y} = 512, 12$ grid points. The solid red lines display the solution calculated for a gas of $N = 7.5\times10^5$ atoms, of equal transverse size but different longitudinal length: $L_x/\ell_0 = 105$, with $N_x = 384$ grid points. Physical parameters have been chosen so that the equilibrium chemical potential is the same for the two configuration and equal to $\mu/\hbar\omega_0 = 2.38$. As expected, the spectra relative to these two configurations are the same. The three curves correspond to modes with zero (Goldstone, black), one (dipole, blue) and two (breathing, green) nodes in the transverse direction. The transverse profile of these modes is reported in panel (b). In panel (a), the light green cross highlights the transverse breathing mode that is excited at early times to simulate the inflaton oscillations; the light blue and grey crosses respectively highlight the dipole and Goldstone modes of opposite momenta that are resonantly excited by the parametric processes indicated by the arrows.

insensitive to the physical dimensions of the system, we adjusted the number of particles in such a way that the density of the system is the same in the two cases (the GPE Hamiltonian defined in Eq. (5) is invariant under the transformation $\psi \to \psi/\sqrt{\lambda}$, $N \to \lambda N$). The spectrum of the system in these two configurations is the same, as expected, except for a difference in the density of eigenstates, due to the different longitudinal lengths (we do not show this feature in Fig. 1(a) as it would be difficult to visualize). Such a different density of eigenstates will result in minor deviation in the results obtained with these two configurations.

4. Numerical method

We model the nonlinear dynamics of the system beyond the Bogoliubov theory by using the truncated Wigner approximation (TWA) [40]. This technique has been used extensively in the literature for studying quantum field effects at the test-field level such as the (analog of the) Hawking radiation emanated from a sonic horizon [10], and even beyond [35, 41, 42]. Within such a semiclassical theory, quantum noise is only encoded in the initial condition of the system while the following evolution is classical and described by the GPE in Eq. (5). The quantum field operator is thus modelled as a classical field $\psi(\mathbf{r})$, whose initial configuration is sampled according to the Wigner quasi-probability distribution that describes the quantum state of the system at the initial time. Formally, the TWA results from neglecting a third-order derivative term from the Fokker-Plank-like equation for the Wigner distribution of the system, that cannot be mapped into a stochastic, classical equation of motion [40].

In our calculations, we take the Bogoliubov vacuum as the initial state of the dynamics. Within the TWA [43], such a state is constructed as the superposition of two contributions:

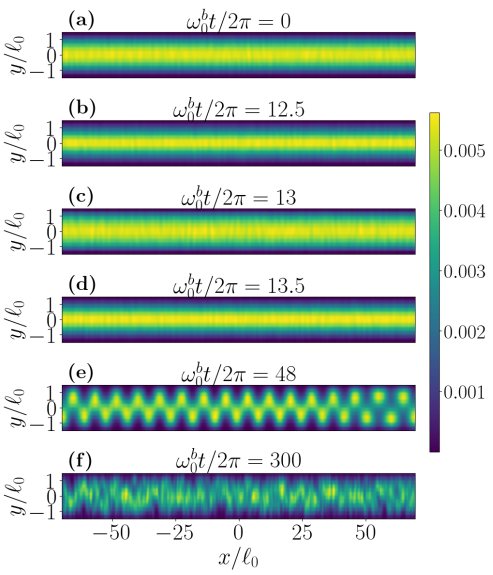

Figure 2. Time evolution of the density profile of a gas of $N = 10^6$ atoms, confined within a box of size $L_{x,y}/\ell_0 = 140, 3.54$ and $N_{x,y} = 512, 12$ grid points with periodic boundary conditions along x. We report the result obtained by propagating in time a single realization of the quantum noise that populates the initial state of the system. (a) Initial condition of the simulation. (b-d) Evolution of the system soon after the initial modulation of the transverse trapping frequency. The resulting transverse breathing oscillations of the cloud are visible. (e) Density profile of the cloud at the time instant when the exponential growth of the population in the resonant dipole and Goldstone modes saturates. Such a profile reveals the macroscopic excitation of the dominant resonant dipole mode. (f) Self-interaction and scattering processes result in a final chaotic state of the system.

one is the order parameter $\varphi_0(\mathbf{r})$ of the condensate at equilibrium, the other is a stochastic component that accounts for the zero-point fluctuations that populate the Bogoliubov vacuum:

$$\psi(\mathbf{r}, t=0) = \varphi_0(\mathbf{r}) + \sum_{\substack{r \\ n \in (+)}} \left(\beta_n^r u_n^r(\mathbf{r}) + \beta_n^{r\,*} v_n^{r\,*}(\mathbf{r})\right) \tag{11}$$

where the sum is restricted to positive norm modes only. The amplitudes β_n^r are independent, zero-mean, Gaussian random variables, that mimic the zero-point fluctuations in each mode according to the semiclassical Wigner representation for the state of a quantum system [44]. These satisfy the following correlation properties: $\langle \beta_k^2 \rangle = \langle (\beta_k^*)^2 \rangle = 0$, $\langle |\beta_k|^2 \rangle = 1/2$. Quantum expectation values of equal time correlators, symmetrically ordered respect to the field operators $\hat{\Psi}$ and $\hat{\Psi}^\dagger$, are obtained as stochastic averages over an ensemble of samples for $\psi(\mathbf{r}, t)$, each relative to a different realization of the initial noise and evolved in time according to the GPE in Eq. (5).

Specifically, we simulate the inflaton oscillations around the bottom of its potential well by exciting the transverse breathing mode of the condensate with zero longitudinal momentum (this is marked in light green in Fig. 1(a)). To this end, we impart an impulsive modulation to the trapping frequency, centred at the time t_0, having the Gaussian form:

$$\omega_0(t)/\omega_0 = 1 + Ae^{-(t-t_0)^2/2\sigma_t^2}. \tag{12}$$

Here, A is the magnitude of the modulation while $\sigma_t = 1/\omega_0^b$ is its duration. In the next section, we study the non-equilibrium dynamics of the condensate after this initial kick. We will investigate the physical processes by which the energy injected in the transverse modes is redistributed into the longitudinal modes, focusing on the early dynamics in order to elucidate the ensuing back-reaction effects.

5. Numerical results for the back-reaction effects

5.1. Parametric amplification and effective friction

We start at $t = 0$ with the system prepared in the Bogoliubov vacuum. In this state, modes are only populated by zero-point fluctuations. An example of the density profile in this configuration is shown in Fig. 2(a). We then give an impulsive modulation to the frequency

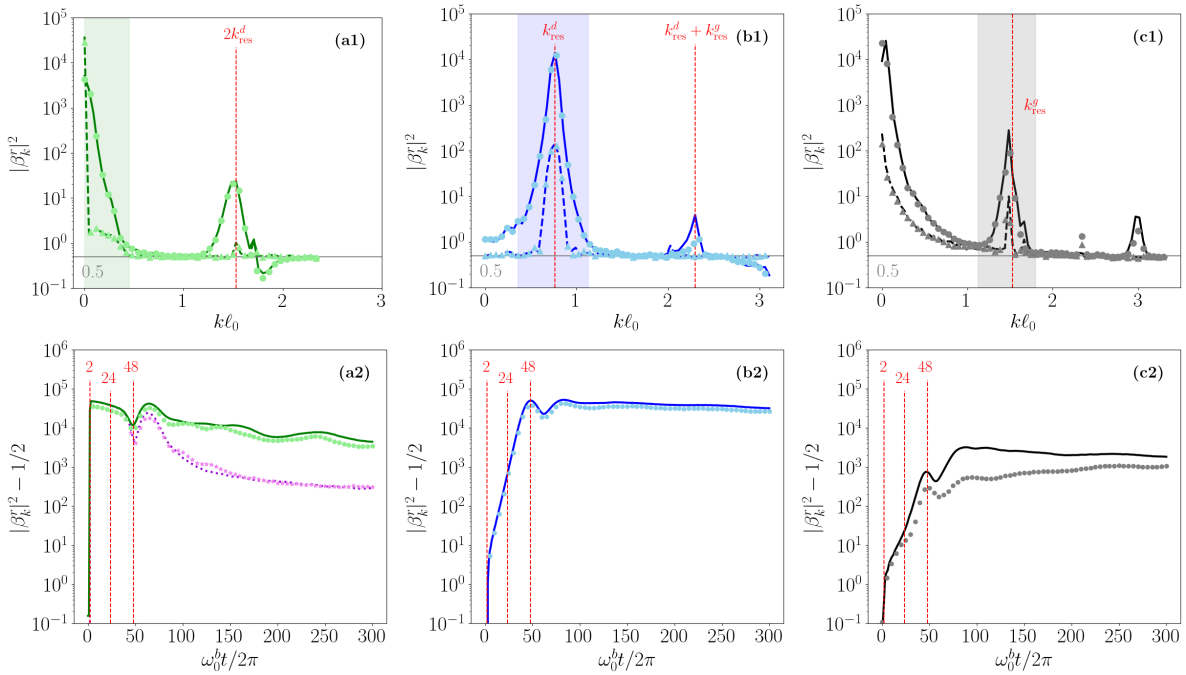

Figure 3. Numerical results of the TWA simulations. Stochastic averages are based on a sample of $\mathcal{N}_r = 1000$ independent realizations. *Panels (a1-c1):* Momentum distribution of the population in the breathing (a1), dipole (b1) and Goldstone (c1) excitation branches, at time $\omega_0^b t/2\pi = 48$ when the saturation of the parametric processes occurs (solid line), and at the intermediate time $\omega_0^b t/2\pi = 24$ (dashed line). Solid and dashed lines show results obtained for the system of longitudinal length $L_x = 140\ell_0$ and $N_x = 512$ grid points. Markers show the corresponding solution calculated for the system with $L_x = 105\ell_0$ and $N_x = 384$. *Panels (a2-c2):* Time-evolution of the integrated population in the breathing (a2), dipole (b2), and Goldstone (c2) branches, over the regions indicated by the shading in the upper panels (the same color code is used in both the upper and lower figures). In (a2), the violet dotted line and markers show the time evolution of the population in the single breathing mode at $k = 0$.

of the transverse trapping potential, of magnitude $A = 10$ and centred at the time $\omega_0 t_0/2\pi = 2$, with the result of setting the system in oscillation in the transverse breathing mode with zero longitudinal momentum. These oscillations are visible in Figs. 2(b-d), where we show the evolution of the density profile soon after the transverse kick. The nonlinear coupling between the Bogoliubov modes, engendered by the interatomic interaction, makes the vacuum fluctuations in the Goldstone and dipole modes parametrically excited by these breathing oscillations. Because of the ring configuration here considered, longitudinal momentum is conserved and parametric down-conversion process involves pairs of particles with opposite momenta as indicated by arrows in Fig. 1(a). Energy conservation makes the parametric processes to be most effective into the Goldstone and dipole modes of frequency $\omega^{g,d}_{\rm res} = \omega^b_0/2$ for which the parametric emission is resonant with the breathing mode oscillations at ω^b_0. Clear evidence of the excitation of the resonant longitudinal modes, in particular the dipole one, is visible in Fig. 2(e). Given the bosonic nature of the Bogoliubov modes, the parametric emission starts from zero-point quantum fluctuations but then gets self-stimulated as the population in the modes increases, leading to a characteristic exponential growth. This amplification process gets distorted when nonlinear effects become relevant, that is when the population in the resonant g, d modes has grown to sizable values, comparable to the population of the driving b mode. This leads to

the saturation of the parametric amplification, as well as to self-interaction, scattering and thermalization processes within the Goldstone and dipole branches, that eventually drive the system into a chaotic thermal state (see Fig. 2(f)).

These dynamics are visible in Fig. 3(a1-c1), where we report a snapshot of the population in the different Bogoliubov modes, $n^r_n(t) + 1/2 \equiv \langle (\hat{b}^r_n)^\dagger \hat{b}^r_n + \hat{b}^r_n (\hat{b}^r_n)^\dagger \rangle /2 = \langle |\beta^r_n(t)|^2 \rangle_W$ at the time when the saturation occurs, and at an intermediate time. We notice the appearance of resonant peaks in both the dipole (b1) and Goldstone (c1) branches, at the values of momenta expected from the analysis of the Bogoliubov spectrum in Fig. 1(a), as well as the emergence at later times of harmonic peaks due to nonlinear processes, at values of momenta fixed by the momentum conservation constrain [35, 45, 46]. The same nonlinear effects are also responsible for the widening of the all visible peaks with time.

The initial exponential growth of the population in the resonant Goldstone and dipole modes is visible in Fig. 3(b2,c2), where we report the evolution of the population integrated within the regions indicated by the shaded areas in Fig. 3(b1,c1). This growth saturates as soon as the populations in the g, d modes have grown to a value comparable to the b mode and nonlinearities have started playing a sizeable effect. When this happens, we see a marked drop in the population in the breathing b branch, as shown in Fig. 3(a2), that is a signal of effective friction experienced by the breathing mode, due to back-reaction effects. Interestingly, such a damping is not purely monotonic, but energy gets at least partially exchanged between the transverse and longitudinal modes. This intermediate-time damped-oscillatory phenomenology is qualitatitively similar to the one predicted in [25, 29] for the back-reaction onto a moving mirror induced by the dynamical Casimir emission, where we demonstrated that a full exchange of energy between the optical field and the mirror is suppressed by purely quantum effects, but, as we are going to see in the next Sections, also displays interesting new features stemming from the many-mode nature of our system.

Finally, it is important to note how Fig. 3 shows results obtained for the two different sizes of the system given in Sec. 3. As expected, such results closely resemble each another, except for minor deviations that we ascribe to the different modes densities and thus resonances pertaining to the two configurations.

5.2. Local observables and de-phasing

The mode-wise analysis developed in the previous section highlighted many interesting dynamical effects: At the early time of the simulation, when the breathing mode is highly excited, we observed the parametric amplification of the vacuum fluctuations in the Goldstone and dipole modes and the simultaneous decay of the population in the transverse breathing mode with an approximately constant damping rate. During this stage of the evolution, the state of the breathing mode closely resembles a classical state and the dynamics is expected to be accurately modelled by approximating the breathing mode with its mean-field component. At later time instead, when the populations in the resonant modes have grown to a value comparable to the breathing mode, nonlinear effects result in the saturation of the parametric processes, generation of harmonic excitations, widening of peaks in the momentum spectrum and, remarkably, in a drastic modification of the qualitative features of the effective damping experienced by the breathing mode.

In this Section, we complement the momentum-space analysis by looking at spatially local quantities which have a direct connection to fluctuations in the system, thus explicitly showing the crucial role of the quantum effects in the back-reaction dynamics. Specifically, we study the spatial correlation function $C_w(X;t)$ of the transverse fluctuations of the cloud, whose transverse size we define as:

$$w(x,t) \equiv \frac{\int_0^{L_y} dy |\psi(\mathbf{r},t)|^2 y^2}{\int_0^{L_y} dy |\psi(\mathbf{r},t)|^2}. \tag{13}$$

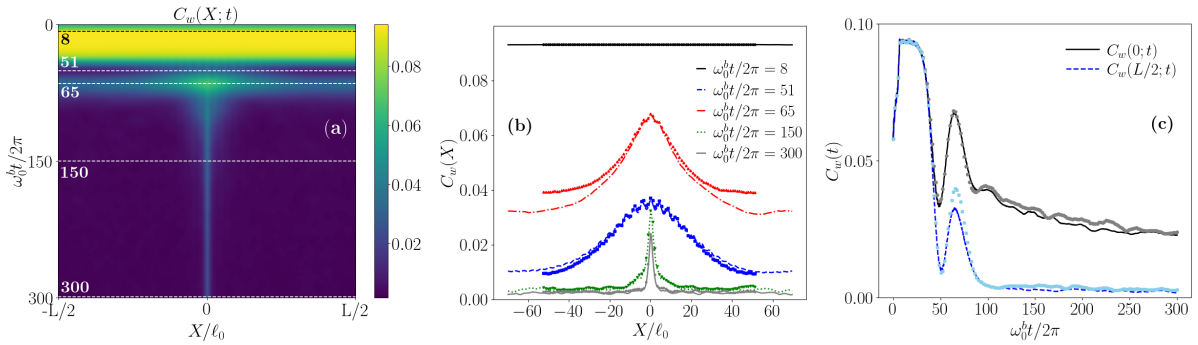

Figure 4. *Left panel:* Time-evolution of the spatial correlation function $C_w(X;t)$ of the transverse size of the cloud, calculated for the system of longitudinal length $L_x = 140\ell_0$ and $N = 10^6$ atoms. *Middle panel:* Cuts of the correlation function at the different times indicated by the horizontal dashed lines in the left panel. *Right panel:* Time evolution of the spatial correlation function for coincident $C_w(0;t)$ and opposite $C_w(L/2;t)$ points around the ring: the former gives information on the total oscillation intensity, while the latter indicates the spatial coherence of the oscillations. As in the previous Figures, lines and markers show the results obtained for the system of longitudinal length $L_x = 140\ell_0$ ($N = 10^6$) and $L_x = 105\ell_0$ ($N = 7.5 \times 10^5$), respectively.

Indicating by $\delta w(x,t) = w(x,t) - \bar{w}(0)$ the x-dependent variation of the transverse size of the cloud respect to the initial spatial average $\bar{w} \equiv L_x^{-1} \int_0^{L_x} dx\, w(x, t=0)$, we define:

$$C_w(X;t) \equiv \left\langle \frac{\delta w(x,t)\delta w(x+X,t)}{\bar{w}^2} \right\rangle_W . \tag{14}$$

The full time evolution of $C_w(X;t)$ is illustrated in Fig. 4(a). Right after the initial kick around $\omega_0^b t = 2$, the system oscillates coherently with a uniform amplitude, so that the correlation function is large and uniform in space. At later time instead, the overall magnitude of C_w decreases as a signature of back-reaction-induced damping, and becomes sharply peaked at $X = 0$ at an even faster rate, which is a clear signal of loss of spatial coherence of the transverse oscillations. Such a de-phasing is a direct effect of the fluctuations in the system: the enhanced fluctuations of the two-mode-squeezed-like state of the emitted g, d fields directly transfer into a analogous fluctuations of the back-reaction-induced friction force. A more quantitative insight into the evolution of the spatial correlation function can be drawn from Fig. 4(b), where we report cuts of Fig. 4(a) at different times. From these plots, we clearly notice that the b mode loses spatial coherence at a much quicker rate compared to the much longer time scale of the decays of the oscillation intensity. A momentum-space signature of this effect was already visible in Fig. 3(a1), as a broadening of the population peak close to zero-momentum in the breathing branch, whose large momentum-width corresponds to the short real-space coherence length. Also for these quantities, we have checked in the Figures that the numerical results are qualitatively identical for systems of different sizes.

The results of this section explicitly demonstrates that fluctuations have dramatic consequences in determining the dynamics of a spatially-extended multi-mode system as the one here considered. In particular, our calculations confirm the outcome of previous studies carried out with simpler optomechanical configurations [29], and prove that mean-field models are expected to fail in accurately describing the physics of the back-reaction.

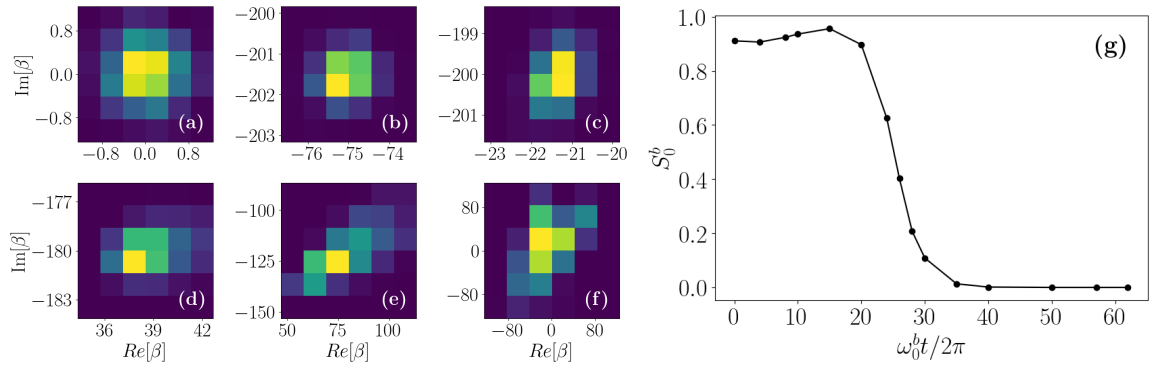

Figure 5. *Panels (a-f):* Phase space Wigner distribution for the transverse breathing mode at zero longitudinal momentum, at the time instants (a) $\omega_0^b t/2\pi = 0$, (b) $\omega_0^b t/2\pi = 10$, (c) $\omega_0^b t/2\pi = 20$, (d) $\omega_0^b t/2\pi = 30$, (e) $\omega_0^b t/2\pi = 40$,(f) $\omega_0^b t/2\pi = 50$. The Wigner function at each time has been reconstructed from the $\mathcal{N}_r = 1000$ samples of the stochastic simulations. We discretized the relevant portion of the phase space by using the number of grid points: $\mathcal{N}_b^R = \mathcal{N}_b^I = \mathcal{N}_r^{1/4} \approx 6$ along both the real and imaginary axes. *Panel (g):* Time evolution of the linear entanglement entropy S_0^b of the breathing mode as defined in the text. At the early time, when the system can be treated semiclassically, the value of the entropy is close to one. At later time instead we observe a drastic decrease of the value of the entropy, which signals entanglement of the breathing mode with the resonant Goldstone and dipole modes.

5.3. Entanglement signatures

In this last section, we further comment on the validity of the TWA that we use to solve for the dynamics of our analog system. The physical significance of the TWA has been long debated within the quantum optics community (see for example [47]), but the implications of this approximation on the dynamics of a quantum system are still not completely understood. Specifically, as detailed in Sec. 4, the TWA is based on a classical evolution of an initial quantum state and it is thus natural to wonder to what extent this formalism is able to capture quantum features of the dynamics of a physical system. While an in-depth study of the physical meaning of the TWA and of its precise limits is an important issue that needs still to be addressed in full detail, we give further evidence in this last section on the capabilities of the TWA to capture at least some features of the quantum dynamics of the system at hand.

To start with, we note that a positive initial Wigner distribution (like the one modelling the Bogoliubov vacuum) remains positive under classical evolution. This entails that quantum states characterized by negative Wigner functions cannot be modelled by the TWA. However, strictly quantum states exist that are described by positive Wigner distributions, such as squeezed states. This means that it is possible in principle that certain quantum features of the dynamics can be captured by working with the TWA. The results presented in the previous sections support this statement, but we give in this section further evidence by studying the entanglement between the zero-momentum transverse breathing mode and the resonant Goldstone and dipole modes. To this end, we use the data from our numerical simulations to construct the Wigner function $W_0^b(\beta, \beta^*)$ for the breathing mode at different time instants (see Fig. 5)(a-f). As entanglement witness, we study the linear entanglement entropy S_0^b of this mode, which is readily evaluated in terms of the corresponding Wigner distribution, as:

$$S_0^b \equiv Tr(\hat{\rho}_{b,0}^2) = \pi \int d^2\beta \, W_{b,0}^2(\beta, \beta^*).$$

In this equation, the integral is performed over the complex phase space of the breathing mode.

In the case of a pure state $S_{b,0} = Tr(\hat{\rho}^2_{b,0}) = Tr(\hat{\rho}_{b,0}) = 1$, while $S_{b,0} < 1$ in case the state is mixed. This latter condition would be a signal of entanglement of the b mode with the resonant g, d modes. At the initial time, the system is in the Bogoliubov vacuum and $S_{b,0} = 1$. We expect that $S_{b,0} \approx 1$ after the transverse kick, as the state of breathing mode can be approximated as a highly excited coherent state with a Gaussian-shaped Wigner distribution (see Fig. 5(b)). At later time instead, when the effect of the back-reaction becomes sizable, the Gaussian shape gets distorted and the Wigner distribution gets broadened [(see]Fig. 5(c-f)], so the value of S^b_0 should drop below one, indicating entanglement. Indeed, this is the behaviour we observe for the linear entropy of the breathing mode, as shown in Fig. 5(g).

These results were obtained by evaluating S^b_0 from the Wigner function of the breathing mode that we reconstructed from our simulations according to Eq.(5.3). The number $\mathcal{N}_r = 1000$ of our samples limits the number $\mathcal{N}_b$ of bins we can use to discretize the complex phase space of the mode: $\mathcal{N}_b = \sqrt{\mathcal{N}_r} = \sqrt{1000} \approx 32$. As closest approximation, we used $\mathcal{N}^R_b = \mathcal{N}^I_b = 6$ to discretize $W^b_0(\beta, \beta^*)$ along the real and imaginary directions. Such a rough grid introduces an error in the result of the numerical integration, which is evident for example in the value of S^b_0 evaluated $t = 0$ in Fig. 5, which deviates from $S^b_0 = 1$ by approximately 0.1. Increasing the precision of the numerical grid by a factor n means increasing the number of numerical samples by a factor n^4, which is out of our numerical capabilities. Despite this error, we clearly see a transition from $S^b_0 \approx 1$ at early time, to $S^b_0 \ll 1$ at later time, as expected.

This result shows that entanglement between the b at $k = 0$ and the g and d resonant modes can be predicted by working within the TWA. Although a clear understanding of the limits of this approximation is still missing, our results demonstrate that the TWA allows to capture features of physics beyond the semiclassical level.

6. Conclusions

In this paper, we give an extended discussion of an analog model of the pre-heating of the early Universe first proposed in Ref.[36]. In our proposal, we make use of a two-dimensional Bose-Einstein condensate of ultra-cold atoms as simulation platform. By working at the level of the truncated Wigner approximation, our numerical results highlight the crucial role of quantum fluctuations in the back-reaction effect of particle production onto the (analog) inflaton field. We observe how the breathing oscillations of the system (which simulate the inflaton degrees-of-freedom) experience an effective damping induced by the parametric emission of excitations in the dipole and Golstone modes (that simulate the matter fields). We highlighted non-trivial dynamical effects beyond the semiclassical level: In particular, we observed a quick fluctuations induced decoherence of the initially in-phase breathing excitation, as well as signature of miltimode entanglement. The generality of the microscopic processes underlying our numerically observed results suggests the importance of going beyond semiclassical approaches [48, 49] and including quantum fluctuation features in the description of back-reaction phenomena in gravitation and cosmology.

7. Acknowledgements

Continuous support from Massimiliano Rinaldi on cosmological issues is most appreciated, as well as enlightening discussions with Stephen Barnett, Miles Blencowe, Bei-Lok Hu and Renaud Parentani. S. B. acknowledges funding from the Leverhulme Trust Grant No. ECF-2019-461, and from University of Glasgow via the Lord Kelvin/Adam Smith (LKAS) Leadership Fellowship. I.C. acknowledges support from the European Union Horizon 2020 research and innovation program under Grant Agreement No. 820392 (PhoQuS) and from the Provincia Autonoma di Trento.

References

[1] Unruh W G 1981 *Phys. Rev. Lett.* **46** 1351–1353
[2] Barceló C, Liberati S and Visser M 2011 *Living Rev. Relativ.* **14**
[3] Faccio D, Belgiorno F, Cacciatori S, Gorini V, Liberati S and Moschella U 2013 *Analogue Gravity Phenomenology Analogue Spacetimes and Horizons, from Theory to Experiment* (Springer)
[4] Hawking S W 1974 *Nature* **248** 30–31
[5] Hawking S W 1975 *Commun. Math. Phys* **43** 199–220
[6] Steinhauer J 2016 *Nat. Phys.* **12** 959–965
[7] de Nova J, Golubkov K, Kolobov V and Steinhauer J 2019 *Nature* **569** 688–691
[8] Kolobov V, Golubkov K, de Nova J and Steinhauer J 2021 *Nat. Phys.* **17** 362–367
[9] Garay L J, Anglin J R, Cirac J I and Zoller P 2000 *Phys. Rev. Lett.* **85** 4643–4647
[10] Carusotto I, Fagnocchi S, Recati A, Balbinot R and Fabbri A 2008 *New J. Phys.* **10** 103001
[11] Eckel S, Kumar A, Jacobson T, Spielman I B and Campbell G K 2018 *Physical Review X* **8** 021021
[12] Steinhauer J, Abuzarli M, Aladjidi T, Bienaimè T amd Piekarski C, Liu W, Giacobino E, Bramati A and Glorieux Q 2022 *Nat. Commun.* **13** 2890
[13] Torres T, Patrick S, Coutant A, Richartz M, Tedford E and Weinfurtner S 2017 *Nat. Phys.* **13** 833–836
[14] Schander S and Thiemann T 2021 *Front. Astron. Space Sci.* **8** 692198
[15] Fischetti M V, Hartle J B and Hu B L 1979 *Phys. Rev. D* **20** 1757–1771
[16] Hartle J B and Hu B L 1979 *Phys. Rev. D* **20** 1772–1782
[17] Hartle J B and Hu B L 1980 *Phys. Rev. D* **21** 2756–2769
[18] Hartle J B 1980 *Phys. Rev. D* **22** 2091–2095
[19] Hartle J B 1981 *Phys. Rev. D* **23** 2121–2128
[20] Hu B L and Verdaguer E 2020 *Semiclassical and Stochastic Gravity: Quantum Field Effects on Curved Spacetime* Cambridge Monographs on Mathematical Physics (Cambridge University Press)
[21] Hu B 2005 *Int. J. Theor. Phys.* **44** 1785–1806
[22] Nation P D and Blencowe M P 2010 *New Journal of Physics* **12** 095013
[23] Ding S, Maslennikov G, Hablützel R and Matsukevich D 2018 *Phys. Rev. Lett.* **121** 130502
[24] Kardar M and Golestanian R 1999 *Rev. Mod. Phys.* **71** 1233–1245
[25] Butera S and Carusotto I 2019 *Phys. Rev. A* **99** 053815
[26] Macrì V, Ridolfo A, Di Stefano O, Kockum A F, Nori F and Savasta S 2018 *Phys. Rev. X* **8** 011031
[27] Dalvit D A R and Maia Neto P A 2000 *Phys. Rev. Lett.* **84** 798–801
[28] Maia Neto P A and Dalvit D A R 2000 *Phys. Rev. A* **62** 042103
[29] Butera S and Carusotto I 2019 *EPL (Europhysics Letters)* **128** 24002
[30] Butera S 2022 *Phys. Rev. D* **105** 016023
[31] Balbinot R, Fagnocchi S, Fabbri A and Procopio G P 2005 *Phys. Rev. Lett.* **94** 161302
[32] Patrick S, Goodhew H, Gooding C and Weinfurtner S 2021 *Phys. Rev. Lett.* **126** 041105
[33] Bain J 2013 *Stud. Hist. Philos. M. P.* **44** 338–345
[34] Bassett B, Tsujikawa S and Wands D 2006 *Rev. Mod. Phys.* **78** 537–589
[35] Robertson S, Michel F and Parentani R 2018 *Phys. Rev. D* **98** 056003
[36] Butera A and Carusotto I 2022 *arXiv:2207.00311*
[37] Dalfovo F, Giorgini S, Pitaevskii L and Stringari S 1999 *Rev. Mod. Phys.* **71** 463–512
[38] Castin Y and Dum R 1998 *Phys. Rev. A* **57** 3008
[39] Gardiner C W 1997 *Phys. Rev. A* **56** 1414
[40] Steel M J, Olsen M K, Plimak L I, Drummond P D, Tan S M, Collett M J, Walls D F and Graham R 1998 *Phys. Rev. A* **58** 4824–4835
[41] Jain P, Weinfurtner S, Visser M and Gardiner C W 2007 *Phys. Rev. A* **76** 033616
[42] Prokopec T and Roos T G 1997 *Phys. Rev. D* **55** 3768–3775
[43] Sinatra A, Lobo C and Castin Y 2001 *Phys. Rev. Lett.* **87** 210404
[44] Walls D F and Milburn G J 2008 *Quantum Optics* (Springer)
[45] Micha R and Tkachev I I 2003 *Phys. Rev. Lett.* **90** 121301
[46] Barroso V S, Geelmuyden A amd Fifer Z, Erne S, Avgoustidis A, Hill R J A and Weinfurtner S 2022 *arXiv:2207.02199*
[47] Reynaud S, Heidmann A, Giacobino E and Fabre C 1992 I quantum fluctuations in optical systems (*Progress in Optics* vol 30) (Elsevier) pp 1–85
[48] Anderson P R, Molina-París C and Sanders D H 2015 *Phys. Rev. D* **92** 083522
[49] Pla S, Newsome I M, Link R S, Anderson P R and Navarro-Salas J 2021 *Phys. Rev. D* **103** 105003